A Mixed Formulation for Nonlinear Analysis of Cable Structures

Miquel Crusells-Girona[a,*], Filip C. Filippou[a], Robert L. Taylor[a]

[a]*Department of Civil and Environmental Engineering. University of California at Berkeley. USA.*

Abstract

This paper proposes a general finite-element procedure for the nonlinear analysis of cables based on a mixed variational formulation in curvilinear coordinates with finite deformations. The formulation accounts for nonlinear elasticity and inelasticity, overcoming the limitation of recent numerical approaches which integrate explicitly the global balance of linear momentum for a linear elastic material with infinitesimal deformations. The formulation uses a weak form of the catenary problem and of the strain-displacement relation to derive a new family of cable finite elements with a continuous or discontinuous axial force field. Several examples from the literature on nonlinear cable analysis are used to validate the proposed formulation for St. Venant - Kirchhoff elastic materials and neo-Hookean materials. These studies show that the proposed formulation captures the displacements and the axial force distribution with high accuracy using a small number of finite elements.

Keywords: cable analysis, nonlinear analysis, mixed finite elements, weak compatibility

1. Introduction

Cable structures are widely used in engineering practice because they offer the advantages of high ultimate strength, flexibility, light weight and prestressing capabilities, among others. Because the behavior of a flexible

*Corresponding author

Email addresses: miquel.crusells@berkeley.edu (Miquel Crusells-Girona), filippou@berkeley.edu (Filip C. Filippou), rlt@berkeley.edu (Robert L. Taylor)

cable is highly nonlinear, significant effort has been invested into developing accurate and economical numerical models for it. These models have evolved from truss elements to elastic elements satisfying the catenary equation. The survey in Tibert (1999) provides a detailed overview of the different models. The following brief comments highlight the main features of the two basic approaches and point out some of their limitations. The simplest approach involves the representation of the cable as a series of straight truss elements. These are often based on linear displacement interpolation functions in the context of infinitesimal-deformation theory (Michalos and Birnstiel, 1962; Jayaraman and Knudson, 1981; Leonard, 1988). The geometric nonlinearity is often accounted for with the corotational formulation (de Borst et al., 2012), involving the transformation of the node kinematic variables under large displacements. These elements suffer from the excessive mesh refinement required to accurately capture the deformed shape and the axial force distribution, especially when using linear shape functions and thus a constant axial force in the element. Also, because these elements are not specifically formulated as cables, they may exhibit a snap-through instability at states of nearly singular stiffness.

To address the excessive mesh refinement limitation of simple truss elements, catenary elements have been proposed. These elements formulate the global balance of linear momentum assuming one-dimensional infinitesimal linear elasticity (Hooke's law) and obtain the deformed shape by explicit integration (Andreu et al., 2006; Yang and Tsay, 2007; Such et al., 2009; Ahmad Abad et al., 2013; Ahmadizadeh, 2013). Such et al. (2009) and Ahmad Abad et al. (2013) also proposed a finite-difference version of this catenary formulation by discretizing the global balance of linear momentum into n segments.

While catenary formulations give more accurate results than truss elements for the same mesh discretization, they also have shortcomings that limit their range of application. First, current catenary elements do not support extension to finite deformations and nonlinear material behavior. Second, these elements assume infinitesimal deformations and integrate the global balance of linear momentum explicitly without distinction between the 2nd Piola-Kirchhoff (2nd PK) and Cauchy representations of the axial force (Gurtin, 1982, Ch.9). Third, this explicit integration does not accommodate a consistent mass matrix for dynamic analysis, limiting such approaches to the use of a lumped mass with the consequence that a large number of elements is required for accuracy (Thai and Kim, 2011). Finally, because of the

assumption of infinitesimal deformations, the distributed loads do not evolve consistently with the cable elongation, resulting in the inaccurate balance of linear momentum in the deformed configuration. To address this problem, *associated catenary elements* (Andreu et al., 2006) impose restrictions of the form $wL = \tilde{w}l$ with w and L the load and length in the reference configuration, and $\tilde{w}$ and l the load and length in the current configuration, respectively.

To address the limitations of truss and catenary cable elements, this study proposes a new formulation for a family of cable finite elements with the following objectives:

- Use finite deformation theory to describe the geometric nonlinearity.
- Solve the balance of linear momentum consistently.
- Accommodate nonlinear elastic material response.
- Can be extended to inelastic material response.
- Develop a robust and versatile finite element implementation to allow its deployment in a general purpose finite element analysis framework.

The presentation starts with the formulation of the cable kinematics under finite deformations in Section 2, and proceeds to derive the principle of virtual work and weak compatibility relation in Section 3. Subsequently, Section 4 presents the finite element implementation of the weak form of the governing equations, and discusses the numerical stability requirements of the formulation. Following a brief discussion of nonlinear elastic material models in Section 6, the presentation sets the stage for the subsequent numerical studies by describing first the solution of the form finding problem with the current formulation in Section 7. Finally, Section 8 assesses the accuracy and numerical convergence characteristics of the proposed elements with the study of cable problems from the literature.

2. Geometry and Kinematics

2.1. Geometric Preliminaries

Figure 1 shows a curve $\mathcal{C}$ representing an idealized cable in three dimensions, with reference Cartesian coordinate system $\{\mathbf{E}_A\}_{A=1}^{3}$.

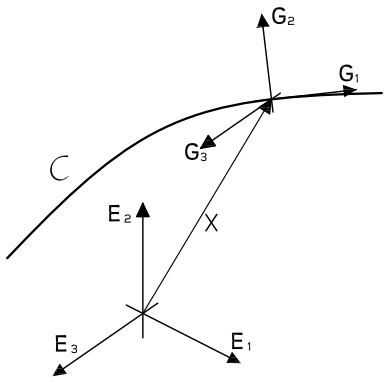

Figure 1: Geometry for general cable.

Define an orthogonal frame $\{\mathbf{G}_i\}_{i=1}^3$ at any material point $P \in \mathcal{C}$ associated with coordinates $\{\xi^i\}_{i=1}^3$ such that

$$\mathbf{G}_1 = \frac{d\mathbf{X}}{d\xi^1} \;\; ; \;\; \mathbf{G}_1 \cdot \mathbf{G}_2 = 0 \;\; ; \;\; \|\mathbf{G}_2\| = 1 \;\; ; \;\; \mathbf{G}_3 = \frac{\mathbf{G}_1 \times \mathbf{G}_2}{\|\mathbf{G}_1 \times \mathbf{G}_2\|} \tag{1}$$

where ξ^1 is the selected parameter for describing the curve. Note that the frame $\{\mathbf{G}_i\}_{i=1}^3$ is orthogonal but, in general, not orthonormal. Indeed, the metric tensor $[G_{ij}]$ for the frame $\{\mathbf{G}_i\}_{i=1}^3$ is of the form

$$[G_{ij}] = [\mathbf{G}_i \cdot \mathbf{G}_j] = \begin{bmatrix} \|\mathbf{G}_1\|^2 & 0 & 0 \\ 0 & 1 & 0 \\ 0 & 0 & 1 \end{bmatrix} \tag{2}$$

Therefore, the differential vector $d\mathbf{X}$ along the curve $\mathcal{C}$ is

$$d\mathbf{X} = \frac{d\mathbf{X}}{d\xi^1} d\xi^1 = \mathbf{G}_1 d\xi^1 \tag{3}$$

The corresponding dual frame $\{\mathbf{G}^i\}_{i=1}^3$ satisfies

$$\mathbf{G}_i = G_{ij}\mathbf{G}^j \quad \Rightarrow \quad \mathbf{G}^i = G^{ij}\mathbf{G}_j = G_{ij}^{-1}\mathbf{G}_j \tag{4}$$

where $[G^{ij}]$ represents the dual metric tensor.

2.2. Finite-Deformation Kinematics

With the preceding definitions, let the cable $\mathcal{C}$ undergo the motion $\boldsymbol{\chi}(\xi^1) : \mathbb{R}^3 \to \mathbb{R}^3$ in Fig. 2, such that $\boldsymbol{\chi}(\mathbf{X}(\xi^1)) = \mathbf{x}$, where $\mathbf{X}$ represents the position vector in the reference configuration $\mathcal{P}_0$ and $\mathbf{x}$, the position vector in the current configuration $\mathcal{P}$. Upper case letters denote the variables in the reference configuration and lower case letters, the variables in the current configuration. Note that the cable motion can be completely described by the single coordinate ξ^1, because the cable is idealized as a one-dimensional manifold (Bishop and Goldberg, 1980).

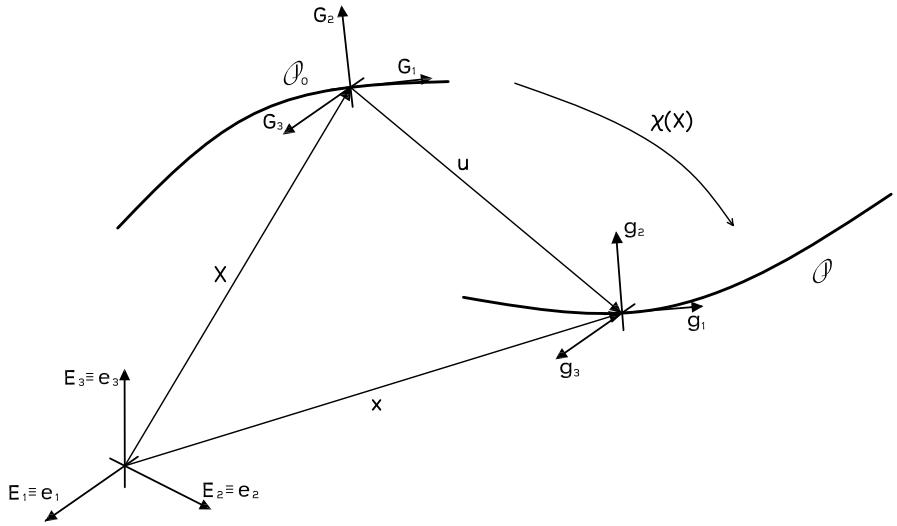

Figure 2: Motion $\mathbf{x} = \boldsymbol{\chi}(\mathbf{X}(\xi^1))$ of the cable $\mathcal{C}$.

In the global Cartesian coordinate system, $\mathbf{X} = X_A \mathbf{E}_A$ defines the reference coordinates, whereas $\mathbf{x} = x_i \mathbf{e}_i$ defines the current coordinates. Note that, in Cartesian coordinates, $\mathbf{E}_A = \mathbf{E}^A$ and $\mathbf{e}_i = \mathbf{e}^i$. Let $\{\mathbf{E}_A\}_{A=1}^3 \equiv \{\mathbf{e}_i\}_{i=1}^3$, for simplicity.

Convecting the curvilinear coordinates $\{\xi^i\}_{i=1}^3$ with basis $\{\mathbf{G}_i\}_{i=1}^3$ into the coordinates $\{\eta^i\}_{i=1}^3$ with basis $\{\mathbf{g}_i\}_{i=1}^3$, the deformation gradient $\mathbf{F}$ and the right Cauchy-Green tensor $\mathbf{C}$ are (Steigmann, 1990)

$$\mathbf{F} = \frac{\partial \mathbf{x}}{\partial \mathbf{X}} = \mathbf{g}_i \otimes \mathbf{G}^i \quad ; \quad \mathbf{C} = \mathbf{F}^t \mathbf{F} = g_{ij}\, \mathbf{G}^i \otimes \mathbf{G}^j \tag{5}$$

Thus, $\mathbf{F}\mathbf{G}_1 = \mathbf{g}_1$ and $\mathbf{G}_1 = \mathbf{F}^{-1}\mathbf{g}_1$. The Green-Lagrange strain tensor $\mathbf{E}$ is

$$\mathbf{E} = \frac{1}{2}(g_{ij} - G_{ij})\,\mathbf{G}^i \otimes \mathbf{G}^j \tag{6}$$

Hence the only nonzero strain arises in the $\mathbf{G}_1$ direction. It is

$$\mathrm{E}_{11} = \frac{1}{2}(\|\mathbf{g}_1\|^2 - \|\mathbf{G}_1\|^2) \tag{7}$$

The relevant stretch λ of the problem in the $\mathbf{G}_1$ direction is

$$\lambda^2 = \left(\frac{ds}{dS}\right)^2 = \frac{d\mathbf{x}\cdot d\mathbf{x}}{d\mathbf{X}\cdot d\mathbf{X}} = \frac{g_{11}}{G_{11}} = \left(\frac{\|\mathbf{g}_1\|}{\|\mathbf{G}_1\|}\right)^2 \tag{8}$$

Consequently,

$$\mathrm{E}_{11} = \frac{1}{2}(\lambda^2 - 1)\|\mathbf{G}_1\|^2 \tag{9}$$

The displacement vector $\mathbf{u}$ depends only on the curvilinear coordinate ξ^1 of the material point $P \in \mathcal{C}$

$$\mathbf{u}(\mathbf{X}(\xi^1)) = \mathbf{x}(\mathbf{X}(\xi^1)) - \mathbf{X}(\xi^1) = u_A(\xi^1)\mathbf{E}_A \tag{10}$$

For the referential displacement gradient $\mathbf{H}$ in curvilinear coordinates, one observes that the only nonzero derivative with respect to $\{\xi^i\}_{i=1}^3$ is

$$\frac{d\mathbf{u}}{d\xi^1} = \frac{d\mathbf{x}}{d\xi^1} - \frac{d\mathbf{X}}{d\xi^1} = \mathbf{g}_1 - \mathbf{G}_1 \tag{11}$$

As a result,

$$\mathbf{H} = \frac{d\mathbf{u}}{d\xi^1} \otimes \mathbf{G}^1 \tag{12}$$

so that the relationship between the Green-Lagrange strain $\mathbf{E}$ and the displacement field $\mathbf{u}$ is

$$\mathbf{E} = \frac{1}{2}\left(\frac{d\mathbf{u}}{d\xi^1} \otimes \mathbf{G}^1 + \mathbf{G}^1 \otimes \frac{d\mathbf{u}}{d\xi^1} + \left|\frac{d\mathbf{u}}{d\xi^1}\right|^2 \mathbf{G}^1 \otimes \mathbf{G}^1\right) \tag{13}$$

The only nonzero component of $\mathbf{E}$ can therefore be expressed as

$$\mathrm{E}_{11} = \frac{d\mathbf{u}}{d\xi^1}\cdot\mathbf{G}_1 + \frac{1}{2}\left|\frac{d\mathbf{u}}{d\xi^1}\right|^2 = \frac{d\mathbf{u}}{d\xi^1}\cdot\left(\mathbf{G}_1 + \frac{1}{2}\frac{d\mathbf{u}}{d\xi^1}\right) = \frac{1}{2}\frac{d\mathbf{u}}{d\xi^1}\cdot(\mathbf{G}_1 + \mathbf{g}_1) \tag{14}$$

It is important to observe that the above Green-Lagrange strain E_{11} is, in general, not physical. Indeed, the constitutive equation cannot be directly expressed as a function of E_{11} since the metric tensor $[G_{ij}]$ is not the identity operator, i.e. $G_{11} = \|\mathbf{G}_1\|^2 \neq 1$ in general. However, one can generate an orthonormal basis by normalizing the vectors $\{\mathbf{G}_i\}_{i=1}^3$ to give $\{\hat{\mathbf{G}}_A\}_{A=1}^3$ with $\hat{\mathbf{G}}_A = \mathbf{G}_i/\|\mathbf{G}_i\|$. Consequently, one can transform the components of $\mathbf{E}$ into meaningful quantities by invoking the change of basis

$$\mathbf{E} = \mathrm{E}_{ij}\mathbf{G}^i \otimes \mathbf{G}^j = \hat{\mathrm{E}}_{AB}\hat{\mathbf{G}}_A \otimes \hat{\mathbf{G}}_B \tag{15}$$

Hence,

$$\hat{\mathrm{E}}_{AB} = \mathrm{E}_{ij}(\hat{\mathbf{G}}_A \cdot \mathbf{G}^i)(\hat{\mathbf{G}}_B \cdot \mathbf{G}^j) \tag{16}$$

noting that $\hat{\mathrm{E}}_{11} = G^{11}\mathrm{E}_{11}$, as $\hat{\mathbf{G}}_1 \cdot \mathbf{G}^1 = \|\mathbf{G}^1\|$.

3. Equilibrium and Principle of Virtual Work

For expressing the equilibrium equation of the cable, let $\mathbf{n}$ denote the axial force in the current configuration, hence a Cauchy representation of the axial force. Observe that the first Piola-Kirchhoff and the Cauchy representations of the axial force coincide for the problem in hand, which does not account for changes in the cross section dimensions.

With reference to Eq. 16, the physical Cauchy stress tensor $\hat{\boldsymbol{\sigma}}$ is given by

$$\hat{\boldsymbol{\sigma}} = \hat{\sigma}^{ij}\hat{\mathbf{g}}_i \otimes \hat{\mathbf{g}}_j \tag{17}$$

Consequently, the Cauchy axial force $\mathbf{n}$ corresponds to

$$\mathbf{n} = A\hat{\sigma}^{11}\hat{\mathbf{g}}_1 \otimes \hat{\mathbf{g}}_1\hat{\mathbf{g}}^1 = A\hat{\sigma}^{11}\hat{\mathbf{g}}_1 = A\hat{\sigma}^{11}\sqrt{g^{11}}\mathbf{g}_1 \tag{18}$$

with magnitudes $\mathbf{n} = \hat{\mathrm{n}}\hat{\mathbf{g}}_1 = \mathrm{n}\mathbf{g}_1$ in both bases, where A is the area of the cross section. With the expression for the physical 2nd Piola-Kirchhoff stress tensor $\hat{\mathbf{S}}$ in the form

$$\hat{\mathbf{S}} = \hat{\mathrm{S}}^{ij}\hat{\mathbf{G}}_i \otimes \hat{\mathbf{G}}_j \tag{19}$$

the 2nd Piola-Kirchhoff axial force $\mathbf{N}$ becomes

$$\mathbf{N} = A\hat{\mathrm{S}}^{11}\hat{\mathbf{G}}_1 \otimes \hat{\mathbf{G}}_1\hat{\mathbf{G}}^1 = A\hat{\mathrm{S}}^{11}\hat{\mathbf{G}}_1 = A\hat{\mathrm{S}}^{11}\sqrt{G^{11}}\mathbf{G}_1 \tag{20}$$

with magnitudes $\mathbf{N} = \hat{\mathrm{N}}\hat{\mathbf{G}}_1 = \mathrm{N}\mathbf{G}_1$ in both bases.

The 2nd Piola-Kirchhoff stress S^{11} is related to the Cauchy stress σ^{11} with the pull-back transformation

$$\mathrm{S}^{11} = J\sigma^{11} = \lambda\sigma^{11} \tag{21}$$

where J is the determinant of the deformation gradient $\mathbf{F}$. Obtaining the physical components of $\mathbf{S}$ and $\boldsymbol{\sigma}$ similarly to Eq. 16 gives

$$\mathbf{N} = AG_{11}\frac{\sqrt{g_{11}}}{\sqrt{G_{11}}}\sigma^{11}\hat{\mathbf{G}}_1 = A\sqrt{G_{11}}\hat{\sigma}^{11}\sqrt{g^{11}}\hat{\mathbf{G}}_1 = \mathrm{n}\sqrt{G_{11}}\hat{\mathbf{G}}_1 \tag{22}$$

Hence,

$$\hat{\mathrm{N}} = \mathrm{n}\sqrt{G_{11}} \iff \mathrm{n} = \hat{\mathrm{N}}\sqrt{G^{11}} \iff \hat{\mathrm{n}} = \lambda\hat{\mathrm{N}} \tag{23}$$

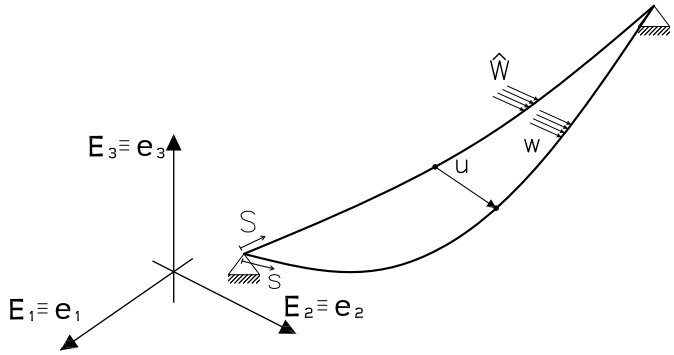

Figure 3: Representation of a cable element.

The global equilibrium of the cable $\mathcal{C}$ in the current configuration in Fig. 3 requires that each component of $\mathbf{n}$ be in equilibrium with the external loads $\mathbf{w}$ expressed per unit of length in the current configuration (Antman, 2005, Ch.3),

$$\mathbf{n}(s) - \mathbf{n}(0) + \int_0^s \mathbf{w}\, ds = \mathbf{0} \tag{24}$$

The local counterpart in Eulerian form can be obtained with the Fundamental Theorem of Calculus

$$\int_0^s \left(\frac{d\mathbf{n}}{ds} + \mathbf{w}\right) ds = \mathbf{0} \tag{25}$$

Hence, by the localization theorem,

$$\frac{d\mathbf{n}}{ds} + \mathbf{w} = \frac{d\left(\hat{\mathrm{n}}\hat{\mathbf{g}}_1\right)}{ds} + \mathbf{w} = \frac{d(\mathrm{n}\mathbf{g}_1)}{ds} + \mathbf{w} = \mathbf{0} \tag{26}$$

This expression arises directly from enforcing equilibrium for a differential cable segment (Lacarbonara, 2013, Ch.3).

The external loads $\mathbf{w}$ can be pulled back to the reference configuration with

$$\mathbf{w}ds = \hat{\mathbf{W}}dS = \mathbf{W}d\xi^1 \tag{27}$$

On account of Eq. 23, the Lagrangian form of the equilibrium equation becomes

$$\frac{d}{dS}\left(\mathrm{n}\mathbf{g}_1\right) + \hat{\mathbf{W}} = \frac{d}{dS}\left(\hat{\mathrm{N}}\sqrt{G^{11}}\mathbf{g}_1\right) + \hat{\mathbf{W}} = \mathbf{0} \tag{28}$$

In summary, if $\hat{\mathrm{N}} = \Psi(\hat{\mathrm{E}})$ is a frame-indifferent constitutive relation (Gurtin, 1982, Ch.7) between the physical Green-Lagrange strain $\hat{\mathrm{E}}$ and the physical 2nd Piola-Kirchhoff axial force $\hat{\mathrm{N}}$, the pair of fields $(\mathbf{u}, \hat{\mathrm{N}})$ will be the solution of the cable problem, if and only if, they satisfy the following equations

$$\begin{cases} G^{11}\dfrac{d\mathbf{u}}{d\xi^1}\cdot\left(\mathbf{G}_1 + \dfrac{1}{2}\dfrac{d\mathbf{u}}{d\xi^1}\right) - \hat{\mathrm{E}} = 0 & \text{in } \Omega = (0, L) \\ \dfrac{d}{dS}\left(\sqrt{G^{11}}\hat{\mathrm{N}}\mathbf{g}_1\right) + \hat{\mathbf{W}} = \mathbf{0} & \text{in } \Omega = (0, L) \\ \hat{\mathrm{N}} - \Psi(\hat{\mathrm{E}}) = 0 & \text{in } \Omega = (0, L) \\ \mathbf{u} = \bar{\mathbf{u}} & \text{on } \Gamma_u \\ \sqrt{G^{11}}\hat{\mathrm{N}}\mathbf{g}_1 = \bar{\mathbf{t}} & \text{on } \Gamma_q \end{cases} \tag{29}$$

for $0 < S < L$ equivalent to $\xi_1^1 < \xi^1 < \xi_2^1$. In these, $\bar{\mathbf{u}}$ and $\bar{\mathbf{t}}$ denote the imposed displacements and boundary forces, respectively. Note that the boundary condition on Γ_q does not represent a prestressing force but a boundary force. In general, this condition is not used in cable problems.

If the pair $(\mathbf{u}, \hat{\mathrm{N}})$ satisfies Eq. 29, then for any variation $\delta\mathbf{u} \in \mathcal{V}$, the space of displacement test functions, and any variation $\delta\hat{\mathrm{N}} \in \mathcal{W}$, the space of test

functions for the 2nd Piola-Kirchhoff axial force, it holds that

$$\begin{cases} \displaystyle\int_0^L \delta\hat{\mathrm{N}} \left\{ G^{11} \frac{d\mathbf{u}}{d\xi^1} \cdot \left(\mathbf{G}_1 + \frac{1}{2} \frac{d\mathbf{u}}{d\xi^1} \right) - \hat{\mathrm{E}} \right\} dS = 0 \\ \displaystyle\int_0^L \delta\mathbf{u} \cdot \left(\frac{d}{dS} \left(\sqrt{G^{11}} \hat{\mathrm{N}} \mathbf{g}_1 \right) + \hat{\mathbf{W}} \right) dS + \left[\delta\mathbf{u} \cdot \left(\bar{\mathbf{t}} - \sqrt{G^{11}} \hat{\mathrm{N}} \mathbf{g}_1 \right) \right]_{\Gamma_q} = 0 \end{cases} \tag{30}$$

with the requirements for spaces $\mathcal{V}$ and $\mathcal{W}$ to be discussed in the following.

Equation 30 corresponds to the two-field weak formulation of Eq. 29. Its solution produces weakly-compatible solutions of the boundary value problem with the constitutive equation imposed strongly.

Regarding the weak form of the strain-displacement relation, sufficient smoothness requirements for $\mathbf{u}$ are $\mathbf{u} \in \mathcal{C}^0(\Omega)$, with $\delta\hat{\mathrm{N}} \in L^2(\Omega)$, so that u_i' has finite jumps at the points with discontinuous derivative and is, therefore, square-integrable.

Regarding the weak form of the equilibrium equation, one can integrate by parts to reduce the order of the highest derivative of the displacement field $\mathbf{u}$: this gives the *Principle of Virtual Work* (PVW) for the cable problem

$$\int_0^L \left(\frac{d(\delta\mathbf{u})}{dS} \cdot \sqrt{G^{11}} \hat{\mathrm{N}} \mathbf{g}_1 \right) dS = \left[\delta\mathbf{u} \cdot \bar{\mathbf{t}} \right]_{\Gamma_q} + \int_0^L \delta\mathbf{u} \cdot \hat{\mathbf{W}} \, dS \tag{31}$$

or, equivalently, integrating over the curvilinear coordinate

$$\int_{\xi_1^1}^{\xi_2^1} \frac{d(\delta\mathbf{u})}{dS} \cdot \hat{\mathrm{N}} \mathbf{g}_1 \, d\xi^1 = \left[\delta\mathbf{u} \cdot \bar{\mathbf{t}} \right]_{\Gamma_q} + \int_{\xi_1^1}^{\xi_2^1} \delta\mathbf{u} \cdot \mathbf{W} \, d\xi^1 \tag{32}$$

This expression can also be derived from the stress-divergence term $\int_\Omega \hat{\mathbf{S}} \cdot \delta\hat{\mathbf{E}} \, d\Omega$ of the general principle of virtual work under finite deformations (Zienkiewicz et al., 2014, Ch.5).

It can be readily concluded that the formulation of the nonlinear catenary problem under finite deformations in curvilinear coordinates can be derived from the following mixed potential $\Pi(\mathbf{u}, \hat{\mathrm{N}})$

$$\Pi(\mathbf{u}, \hat{\mathrm{N}}) = \int_0^L \left(\hat{\mathrm{N}} G^{11} \frac{d\mathbf{u}}{d\xi^1} \cdot \left(\mathbf{G}_1 + \frac{1}{2} \frac{d\mathbf{u}}{d\xi^1} \right) - \chi(\hat{\mathrm{N}}) \right) dS - \int_0^L \mathbf{u} \cdot \hat{\mathbf{W}} \, dS - [\mathbf{u} \cdot \bar{\mathbf{t}}]_{\Gamma_q} \tag{33}$$

where $\chi(\hat{\mathrm{N}})$ is the complementary energy per unit reference length of the material model with constitutive relation $\hat{\mathrm{E}} = d\chi / d\hat{\mathrm{N}}$.

The spaces for the trial solutions of the displacements and the axial forces, $\mathcal{S}$ and $\mathcal{N}$, respectively, become

$$\begin{aligned}\mathcal{S} &= \{\mathbf{u} \in H^1(0,L) \,|\, \mathbf{u} = \bar{\mathbf{u}} \text{ on } \Gamma_u\} \\ \mathcal{N} &= \left\{\hat{\mathrm{N}} \in H^0(0,L) \,|\, \hat{\mathrm{N}} > 0, \text{ and } \hat{\mathrm{N}} = g^{11}\sqrt{G_{11}}\bar{\mathbf{t}} \cdot \mathbf{g}_1 \text{ on } \Gamma_q\right\}\end{aligned} \tag{34}$$

Similarly, the spaces for the test functions of the displacements and the axial forces, $\mathcal{V}$ and $\mathcal{W}$, respectively, become

$$\begin{aligned}\mathcal{V} &= \{\delta\mathbf{u} \in H^1(0,L) \,|\, \delta\mathbf{u} = 0 \text{ on } \Gamma_u\} \\ \mathcal{W} &= \{\delta\hat{\mathrm{N}} \in H^0(0,L) \,|\, \delta\hat{\mathrm{N}} = 0 \text{ on } \Gamma_q\}\end{aligned} \tag{35}$$

where $H^k(\Omega)$ represents the Sobolev space for the $k-$th weak derivative in the $L^2(\Omega)$ norm (Evans, 2010, Ch.5)

Note that there are no continuity requirements for the axial force field $\hat{\mathrm{N}}$ according to Eqs. 34 and 35. Consequently, it is possible to explore cable finite element formulations with continuous or discontinuous axial force distributions.

4. Finite Element Implementation

The discretization of the governing equations requires interpolations for $\hat{\mathrm{N}}(\xi^1)$ and $\mathbf{u}(\xi^1) = (u_1(\xi^1), u_2(\xi^1), u_3(\xi^1))$. In general, different interpolation functions are possible for the two independent fields in a mixed finite element formulation (Zienkiewicz et al., 2014, Ch.2).

For $\hat{\mathrm{N}}(\xi^1)$, consider a k-th order Galerkin approximation of the form

$$\hat{\mathrm{N}}(\xi^1) = \sum_{i=1}^{k+1} \varphi_i(\xi^1)\hat{\mathrm{N}}_i \;\; ; \;\; \delta\hat{\mathrm{N}}(\xi^1) = \sum_{i=1}^{k+1} \varphi_i(\xi^1)\delta\hat{\mathrm{N}}_i \tag{36}$$

with a vector representation in the form

$$\hat{\mathrm{N}} = \underbrace{\left\{\begin{array}{cccc}\varphi_1 & \varphi_2 & \cdots & \varphi_{k+1}\end{array}\right\}}_{\boldsymbol{\varphi}^t} \underbrace{\left\{\begin{array}{c}\hat{\mathrm{N}}_1 \\ \hat{\mathrm{N}}_2 \\ \vdots \\ \hat{\mathrm{N}}_{k+1}\end{array}\right\}}_{\hat{\mathbf{N}}} = \boldsymbol{\varphi}^t\hat{\mathbf{N}} = \hat{\mathbf{N}}^t\boldsymbol{\varphi} \tag{37}$$

where $\boldsymbol{\varphi}$ and $\hat{\mathbf{N}}$ are $(k+1)\times 1$ arrays.

For $\mathbf{u}(\xi^1)$, consider an l-th order Galerkin approximation of the form

$$\mathbf{u}(\xi^1) = \sum_{i=1}^{l+1} \phi_i(\xi^1)\mathbf{u}_i \;\; ; \;\; \delta\mathbf{u}(\xi^1) = \sum_{i=1}^{l+1} \phi_i(\xi^1)\delta\mathbf{u}_i \tag{38}$$

with a vector representation in three dimensions of the form

$$\mathbf{u} = \underbrace{\begin{bmatrix} \phi_1 & 0 & 0 & \cdots & \phi_{l+1} & 0 & 0 \\ 0 & \phi_1 & 0 & \cdots & 0 & \phi_{l+1} & 0 \\ 0 & 0 & \phi_1 & \cdots & 0 & 0 & \phi_{l+1} \end{bmatrix}}_{\boldsymbol{\phi}^t} \underbrace{\begin{Bmatrix} u_1^1 \\ u_1^2 \\ u_1^3 \\ \vdots \\ u_{l+1}^1 \\ u_{l+1}^2 \\ u_{l+1}^3 \end{Bmatrix}}_{\hat{\mathbf{u}}} = \begin{bmatrix} \boldsymbol{\phi}_1^t \\ \boldsymbol{\phi}_2^t \\ \boldsymbol{\phi}_3^t \end{bmatrix} \hat{\mathbf{u}} = \boldsymbol{\phi}^t\hat{\mathbf{u}} \tag{39}$$

In this case, $\boldsymbol{\phi}$ is an $n(l+1)\times n$ array, while $\hat{\mathbf{u}}$ is an $n(l+1)\times 1$ array, with n the dimension of the problem. Using the same shape functions for the reference configuration, $\mathbf{X} = \boldsymbol{\phi}^t\hat{\mathbf{X}}$, the current configuration results from

$$\mathbf{x} = \mathbf{X} + \mathbf{u} = \boldsymbol{\phi}^t(\hat{\mathbf{X}} + \hat{\mathbf{u}}) = \boldsymbol{\phi}^t\hat{\mathbf{x}} \tag{40}$$

With these interpolation functions, the weak form of the compatibility equation over the domain Ω_e of an element becomes

$$\int_{\Omega_e} \delta\hat{\mathbf{N}}^t\boldsymbol{\varphi}\left(G^{11}\hat{\mathbf{u}}^t\boldsymbol{\phi}'\left(\mathbf{G}_1 + \frac{1}{2}(\boldsymbol{\phi}')^t\hat{\mathbf{u}}\right) - \hat{\mathrm{E}}(\hat{\mathbf{N}})\right) dS = 0 \tag{41}$$

where $(\cdot)'$ denotes the derivative with respect to the curvilinear coordinate ξ^1. Note that Eq. 41 requires the strong enforcement of a constitutive relation in the form of $\hat{\mathrm{E}} = \Psi^{-1}(\hat{\mathrm{N}}) = \hat{\Psi}^{-1}(\hat{\mathbf{N}})$.

Likewise, the weak form of the equilibrium equation over the domain Ω_e of an element becomes

$$\int_{\Omega_e} \delta\hat{\mathbf{u}}^t\boldsymbol{\phi}'\, G^{11}\boldsymbol{\varphi}^t\hat{\mathbf{N}}\hat{\mathbf{g}}\, dS = [\delta\hat{\mathbf{u}}^t\boldsymbol{\phi}\,\bar{\mathbf{t}}]_{\partial\Omega_e} + \int_{\Omega_e} \delta\hat{\mathbf{u}}^t\boldsymbol{\phi}\,\hat{\mathbf{W}}\, dS \tag{42}$$

where $\hat{\mathbf{g}} = \mathbf{G}_1 + (\boldsymbol{\phi}')^t\hat{\mathbf{u}}$ is the numerical counterpart to $\mathbf{g}_1$.

The absence of a derivative of the axial force $\hat{\mathrm{N}}$ in Eqs. 41 and 42 permits the exploration of a continuous and a discontinuous representation of the axial force for the cable, as discussed in the following.

4.1. Mixed Cable Element with Continuous Axial Force

For the element with continuous axial force representation, the cable is subdivided into e elements with k-th order interpolation for the axial forces and l-th order interpolation for the displacements.

Equations 41 and 42 constitute a nonlinear system of $n(l+1)+k+1$ equations with $n(l+1)+k+1$ unknowns, which can be solved with any suitable iterative solution strategy such as the Newton-Raphson method. For this purpose, it is required to establish the consistent linearization of the *expanded* stress-divergence term $\mathbf{R} = (\mathbf{R}_1, \mathbf{R}_2)$ with components

$$\begin{aligned} \mathbf{R}_1(\hat{\mathbf{N}}, \hat{\mathbf{u}}) &= \int_{\Omega_e} \boldsymbol{\varphi} \left(G^{11} \hat{\mathbf{u}}^t \boldsymbol{\phi}' \left(\mathbf{G}_1 + \frac{1}{2} (\boldsymbol{\phi}')^t \hat{\mathbf{u}} \right) - \hat{\mathrm{E}}(\hat{\mathbf{N}}) \right) dS \\ \mathbf{R}_2(\hat{\mathbf{N}}, \hat{\mathbf{u}}) &= \int_{\Omega_e} G^{11} \boldsymbol{\varphi}^t \hat{\mathbf{N}} \, \boldsymbol{\phi}' \hat{\mathbf{g}} \, dS \end{aligned} \tag{43}$$

Assuming that $\mathbf{R}(\hat{\mathbf{N}}, \hat{\mathbf{u}}) \equiv \mathbf{R}(\mathbf{V})$ and linearizing at the point $\bar{\mathbf{V}} = (\hat{\mathbf{N}}, \hat{\mathbf{u}})$ gives

$$\mathcal{L}\mathbf{R}(\bar{\mathbf{V}}, \Delta\mathbf{V}) = \mathbf{R}|_{\bar{\mathbf{V}}} + \underbrace{\left. \frac{\partial \mathbf{R}}{\partial \mathbf{V}} \right|_{\bar{\mathbf{V}}} (\mathbf{V} - \bar{\mathbf{V}})}_{\mathrm{D}\mathbf{R}(\bar{\mathbf{V}}, \Delta\mathbf{V})} \tag{44}$$

noting that $\bar{\mathbf{V}}$ is an $n(l+1)+k+1$-dimensional vector.

The Fréchet derivative at $\bar{\mathbf{V}}$ for the consistent linearization represents the *expanded stiffness* of the element in the form of an $n(l+1)+k+1 \times n(l+1)+k+1$ array

$$\mathbf{K} = \left. \frac{\partial \mathbf{R}}{\partial \mathbf{V}} \right|_{\bar{\mathbf{V}}} = \begin{bmatrix} \mathbf{K_{NN}} & \mathbf{K_{Nu}} \\ \mathbf{K_{uN}} & \mathbf{K_{uu}} \end{bmatrix} = \begin{bmatrix} \dfrac{\partial \mathbf{R}_1}{\partial \hat{\mathbf{N}}} & \dfrac{\partial \mathbf{R}_1}{\partial \hat{\mathbf{u}}} \\ \dfrac{\partial \mathbf{R}_2}{\partial \hat{\mathbf{N}}} & \dfrac{\partial \mathbf{R}_2}{\partial \hat{\mathbf{u}}} \end{bmatrix} \tag{45}$$

with the following components

$$\begin{aligned}
\mathbf{K_{NN}} &= \frac{\partial \mathbf{R}_1}{\partial \hat{\mathbf{N}}} = -\int_{\Omega_e} \boldsymbol{\varphi} \frac{\partial \hat{\mathrm{E}}}{\partial \hat{\mathbf{N}}}\, dS = -\int_{\Omega_e} \boldsymbol{\varphi} \frac{\partial \hat{\mathrm{E}}}{\partial \hat{\mathrm{N}}} \boldsymbol{\varphi}^t\, dS \\
\mathbf{K_{Nu}} &= \frac{\partial \mathbf{R}_1}{\partial \hat{\mathbf{u}}} = \int_{\Omega_e} G^{11} \boldsymbol{\varphi} \hat{\mathbf{g}}^t (\boldsymbol{\phi}')^t dS \\
\mathbf{K_{uN}} &= \frac{\partial \mathbf{R}_2}{\partial \hat{\mathbf{N}}} = \int_{\Omega_e} G^{11} \boldsymbol{\phi}' \hat{\mathbf{g}} \boldsymbol{\varphi}^t\, dS \\
\mathbf{K_{uu}} &= \frac{\partial \mathbf{R}_2}{\partial \hat{\mathbf{u}}} = \int_{\Omega_e} G^{11} \boldsymbol{\varphi}^t \hat{\mathbf{N}} \boldsymbol{\phi}' (\boldsymbol{\phi}')^t dS
\end{aligned} \tag{46}$$

$\mathbf{K_{NN}}$ and $\mathbf{K_{uu}}$ are symmetric. Moreover, $\mathbf{K_{Nu}} = \mathbf{K}_{\mathbf{uN}}^t$, so that the expanded stiffness $\mathbf{K}$ of the mixed cable element is also symmetric, as can be expected from the existence of the potential in Eq. 33.

4.2. Mixed Cable Element with Discontinuous Axial Force

For the element with discontinuous axial force representation, the cable is subdivided into e elements with k-th order interpolation for the axial forces and l-th order interpolation for the displacements, identical to the element with continuous representation. In this case, however, the axial forces are treated as internal degrees of freedom rather than as global, and are consequently condensed out at the element level before assembly of the element response. This results in two independent axial force values at the node shared by two adjacent elements, when noting that the strain-displacement relation in Eq. 41 does not involve derivatives of $\hat{\mathrm{N}}$, so that $\hat{\mathrm{N}} \in H^0(0, L)$. This permits a discontinuity in the axial force distribution. The resisting force of the element $\mathbf{R}(\hat{\mathbf{N}}, \hat{\mathbf{u}})$ is then of the form $\mathbf{R}(\hat{\mathbf{N}}(\hat{\mathbf{u}}), \hat{\mathbf{u}})$ with the axial force values $\hat{\mathbf{N}}$ determined in each element. The stress-divergence term is

$$\mathbf{R}(\hat{\mathbf{N}}(\hat{\mathbf{u}}), \hat{\mathbf{u}}) = \int_{\Omega_e} G^{11} \boldsymbol{\varphi}^t \hat{\mathbf{N}}\, \boldsymbol{\phi}' \hat{\mathbf{g}}\, dS \tag{47}$$

The strain-displacement relation is enforced within each element in the form

$$\int_{\Omega_e} \boldsymbol{\varphi} \hat{\mathrm{E}}(\hat{\mathbf{N}}) dS = \int_{\Omega_e} \boldsymbol{\varphi} G^{11} \hat{\mathbf{u}}^t \boldsymbol{\phi}' \left(\mathbf{G}_1 + \frac{1}{2} (\boldsymbol{\phi}')^t \hat{\mathbf{u}} \right) dS \tag{48}$$

which gives a set of equations that can be solved iteratively for the axial forces $\hat{\mathbf{N}}$. If $\hat{\mathrm{E}}(\hat{\mathbf{N}})$ is linear in $\hat{\mathbf{N}}$, the determination of the axial forces is rather straightforward from the linear system of equations in Eq. 48.

The consistent linearization of the stress-divergence term gives

$$\mathcal{L}\mathbf{R}(\bar{\mathbf{u}}, \Delta\hat{\mathbf{u}}) = \mathbf{R}|_{\bar{\mathbf{u}}} + \underbrace{\left.\frac{\partial \mathbf{R}}{\partial \hat{\mathbf{u}}}\right|_{\bar{\mathbf{u}}} (\hat{\mathbf{u}} - \bar{\mathbf{u}})}_{\mathrm{D}\mathbf{R}(\bar{\mathbf{u}}, \Delta\hat{\mathbf{u}})} \tag{49}$$

where the Fréchet derivative representing the element stiffness can be derived from

$$\mathbf{K_{NN}}\Delta\hat{\mathbf{N}} + \mathbf{K_{Nu}}\Delta\hat{\mathbf{u}} = 0 \quad \Rightarrow \quad \Delta\hat{\mathbf{N}} = -\mathbf{K}_{\mathbf{NN}}^{-1}\mathbf{K_{Nu}}\Delta\hat{\mathbf{u}} \tag{50}$$

Consequently,

$$\mathrm{D}\mathbf{R}(\bar{\mathbf{u}}, \Delta\hat{\mathbf{u}}) = \underbrace{(\mathbf{K_{uu}} - \mathbf{K_{uN}}\mathbf{K}_{\mathbf{NN}}^{-1}\mathbf{K_{Nu}})}_{\mathbf{K}_{sc}}\Delta\hat{\mathbf{u}} \tag{51}$$

with the stiffness contributions $\mathbf{K_{NN}}$, $\mathbf{K_{uu}}$ and $\mathbf{K_{Nu}}$ in Eq. 46. Because of the symmetry of $\mathbf{K_{uu}}$ and $\mathbf{K_{NN}}$, and $\mathbf{K_{Nu}} = \mathbf{K}_{\mathbf{uN}}^{t}$, the stiffness matrix $\mathbf{K}_{sc}$ for the cable element with discontinuous axial force representation is symmetric.

The discontinuous axial force distribution is suitable for accommodating the application of concentrated forces in cables, as will be discussed in the numerical studies in Section 8.

5. Stability Considerations

The mixed formulation of the nonlinear catenary problem with the displacements $\hat{\mathbf{u}}$ and axial forces $\hat{\mathbf{N}}$ as independent fields results in the following system of equations

$$\underbrace{\begin{bmatrix} \mathbf{K_{NN}} & \mathbf{K_{Nu}} \\ \mathbf{K}_{\mathbf{Nu}}^{t} & \mathbf{K_{uu}} \end{bmatrix}}_{\mathbf{K}(\mathbf{V})} \underbrace{\begin{bmatrix} \Delta\hat{\mathbf{N}} \\ \Delta\hat{\mathbf{u}} \end{bmatrix}}_{\mathbf{V}} = \underbrace{\begin{bmatrix} \mathbf{F}_1 \\ \mathbf{F}_2 \end{bmatrix}}_{\mathbf{b}} \tag{52}$$

where $\mathbf{K}(\mathbf{V}) \equiv \mathbf{K}(\hat{\mathbf{u}}, \hat{\mathbf{N}})$ is symmetric. This problem corresponds to the compressible Stokes problem (Hughes, 2000, Sec.4.3) and a mathematical discussion of the numerical stability for it is presented in Brezzi and Bathe (1990).

Noting that

$$\mathbf{K_{NN}}\Delta\hat{\mathbf{N}} + \mathbf{K_{Nu}}\Delta\hat{\mathbf{u}} = \mathbf{F}_1 \;\; ; \;\; \mathbf{K}_{\mathbf{Nu}}^{t}\Delta\hat{\mathbf{N}} + \mathbf{K_{uu}}\Delta\hat{\mathbf{u}} = \mathbf{F}_2 \tag{53}$$

gives

$$\Delta\hat{\mathbf{u}} = \mathbf{K}_{\mathbf{uu}}^{-1}(\mathbf{F}_2 - \mathbf{K}_{\mathbf{Nu}}^{t}\Delta\hat{\mathbf{N}}) \tag{54}$$

and consequently,

$$\underbrace{(\mathbf{K}_{\mathbf{NN}} - \mathbf{K}_{\mathbf{Nu}}\mathbf{K}_{\mathbf{uu}}^{-1}\mathbf{K}_{\mathbf{Nu}}^{t})}_{\mathbf{\Xi}}\Delta\hat{\mathbf{N}} = \mathbf{F}_1 - \mathbf{K}_{\mathbf{Nu}}\mathbf{K}_{\mathbf{uu}}^{-1}\mathbf{F}_2 \tag{55}$$

If a mode $\hat{\mathbf{N}}$ exists such that $\mathbf{\Xi}\Delta\hat{\mathbf{N}} = \mathbf{0}$, the solution will not be unique and instabilities will arise in the form of spurious modes for the axial forces. To avoid this, it is required that

$$\ker(\mathbf{\Xi}) = \mathbf{0} \tag{56}$$

The same considerations hold for the condensed stiffness matrix $\mathbf{K}_{sc}$ in Eq. 51, leading to the requirement that

$$\ker(\mathbf{K}_{sc}) = \mathbf{0} \tag{57}$$

While these conditions are satisfied for elastic materials, because of the existence of a one-to-one relationship between stress and strain, they may not be satisfied for general inelastic materials. Further details are available in Simo and Hughes (1998) and Zienkiewicz et al. (2014).

6. Material Models

The proposed formulation for the nonlinear analysis of cables supports any constitutive relation of the form $\hat{\mathrm{E}} = \Psi^{-1}(\hat{\mathrm{N}})$. In the context of elastic material behavior two models are relevant: a St Venant-Kirchhoff elastic material as an extension of linear elasticity to finite deformations, and a compressible neo-Hookean material. A brief description of these materials is provided below. Additional information can be found in Zienkiewicz et al. (2014, Ch.6).

6.1. St Venant - Kirchhoff Elastic Material

For a St Venant-Kirchhoff elastic material, the stored energy $\mathcal{U}$ can be expressed in terms of the stretch λ as

$$\mathcal{U}(\lambda) = \frac{E}{8}\left(\lambda^2 - 1\right)^2 \tag{58}$$

where E represents the Young modulus under finite-deformation.

The second Piola-Kirchhoff stress becomes

$$\hat{\mathrm{S}} = \frac{d\mathcal{U}}{d\hat{\mathrm{E}}} = \frac{\partial \mathcal{U}}{\partial \lambda}\frac{\partial \lambda}{\partial \hat{\mathrm{E}}} = \frac{E}{2}(\lambda^2 - 1) = E\,\hat{\mathrm{E}} \tag{59}$$

and the constitutive relation between the second Piola-Kirchhoff axial force and the Green-Lagrange strain can be written as

$$\hat{\mathrm{N}} - \hat{\mathrm{N}}_0 = (EA)\hat{\mathrm{E}} \tag{60}$$

where A is the cross-sectional area and $\hat{\mathrm{N}}_0$ the prestressing force. If the cross-sectional stiffness is independent of the axial force,

$$\frac{\partial \hat{\mathrm{E}}}{\partial \hat{\mathbf{N}}} = \frac{\partial \hat{\mathrm{E}}}{\partial \hat{\mathrm{N}}}\frac{\partial \hat{\mathrm{N}}}{\partial \hat{\mathbf{N}}} = \frac{\boldsymbol{\varphi}^t}{EA} \tag{61}$$

For St Venant-Kirchhoff elastic materials, $\hat{\mathrm{n}} - \hat{\mathrm{n}}_0 = \lambda(\hat{\mathrm{N}} - \hat{\mathrm{N}}_0) \to +\infty$ as $\lambda \to +\infty$. Nevertheless, it is important to note that these elastic materials may misbehave because $\hat{\mathrm{N}} - \hat{\mathrm{N}}_0$ is finite for $\lambda = 0$ (Eq. 59). Also, the model is single-valued in tension, as desired.

6.2. Compressible Neo-Hookean Elastic Material

In a compressible neo-Hookean material model, the stored energy $\mathcal{U}$ is related to the stretch λ as

$$\mathcal{U}(\lambda) = E\left(\frac{1}{4}(\lambda^2 - 1) - \frac{1}{2}\ln\lambda\right) \tag{62}$$

In this case, the second Piola-Kirchhoff stress becomes

$$\hat{\mathrm{S}} = \frac{d\mathcal{U}}{d\hat{\mathrm{E}}} = \frac{\partial \mathcal{U}}{\partial \lambda}\frac{\partial \lambda}{\partial \hat{\mathrm{E}}} = \frac{E}{2}\left(1 - \frac{1}{\lambda^2}\right) \tag{63}$$

The constitutive relation for the second Piola-Kirchhoff axial force can be expressed in terms of the stretch by

$$\hat{\mathrm{N}} - \hat{\mathrm{N}}_0 = \frac{EA}{2}\left(1 - \frac{1}{\lambda^2}\right) \tag{64}$$

It is important to note that, for compressible neo-Hookean elastic materials, $\hat{\mathrm{n}} - \hat{\mathrm{n}}_0 = \lambda(\hat{\mathrm{N}} - \hat{\mathrm{N}}_0) \to +\infty$ as $\lambda \to +\infty$ and that $\hat{\mathrm{N}} - \hat{\mathrm{N}}_0 \to -\infty$ as $\lambda \to 0$, as

desired. Moreover, if the cross-sectional stiffness is independent of the axial force,

$$\frac{\partial \hat{\mathrm{E}}}{\partial \hat{\mathbf{N}}} = \frac{\partial \hat{\mathrm{E}}}{\partial \lambda}\frac{\partial \lambda}{\partial \hat{\mathrm{N}}}\frac{\partial \hat{\mathrm{N}}}{\partial \hat{\mathbf{N}}} = \frac{\lambda^4}{EA}\boldsymbol{\varphi}^t \tag{65}$$

As is the case for the St Venant-Kirchhoff model, the compressible neo-Hookean model is single-valued for tension.

7. Form Finding

At the start of the analysis for a cable, a shape finding or form finding problem arises on account of the fact that typically the initial length of the cable and the span between supports is specified.

The form finding problem is addressed in several studies to date and an overview of prevailing methods for it is available in Veenendaal and Block (2012). Most commonly, two methods are used involving the following procedure:

1. Release some degrees of freedom at the fixed supports and impose appropriate support displacements to obtain the desired span, either statically as a boundary condition (*stiffness matrix methods*), or dynamically in a pseudo-time approach (*dynamic equilibrium methods*) (Argyris et al., 1974).
2. Apply a constraint for imposing the known length of the cable and derive the corresponding extension of the stiffness matrix (Haber and Abel, 1982a,b) (*geometric stiffness methods*).

The present study uses the former method by Argyris et al. (1974) in a static manner, as illustrated in Fig. 4 for a simple cable net with a plane reference configuration. This approach is always possible for cables, because these are modeled as one-dimensional manifolds. In general, it may be difficult to establish the displacement field of a flat reference configuration for the desired span. However, because the proposed formulation assumes a general reference configuration, the adopted procedure is also suitable for any non-flat initial shape, thus making it easier to find such a displacement field.

8. Numerical Studies

The proposed formulation is implemented in two cable elements, one with continuous axial force distribution and another with discontinuous. These

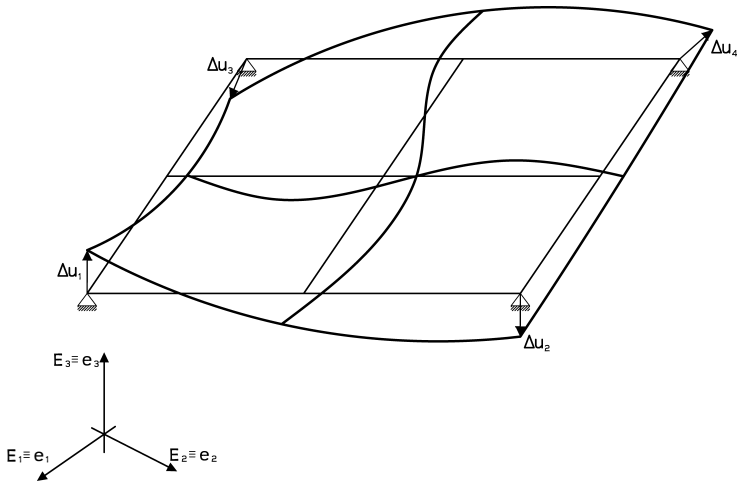

Figure 4: Form finding strategy according to Argyris et al. (1974).

elements are deployed in the general purpose finite element program FEAP (Taylor, 2014) and in the Matlab toolbox FEDEASLab (Filippou, 2007) for conducting the following numerical studies. The elements use a linear approximation for the axial forces ($k = 1$) and a quadratic approximation for the displacements ($l = 2$). Fig. 5 depicts the Lagrange polynomials for the interpolation functions of the element that results in eight degrees of freedom (DOFs), six displacement DOFs, which are depicted with ◯, and two axial force DOFs, which are depicted with •.

The proposed elements are used to investigate three cable examples from the literature, as discussed in the following. For the element with continuous axial force distribution, an initial guess for the axial force and the displacements is required. For the element with a discontinuous axial force distribution, only an initial guess for the displacements is required, as will be discussed for each example.

8.1. 1. Example: Cable under Self-Weight

The simplest model for study consists of a horizontal cable under its own weight. Fig. 6 and Table 1 list the geometric and material properties of the cable that was previously studied in Tibert (1999); Andreu et al. (2006); Thai and Kim (2011); Ahmad Abad et al. (2013). Following Argyris et al. (1974), the deformed shape is obtained by assuming a straight horizontal reference

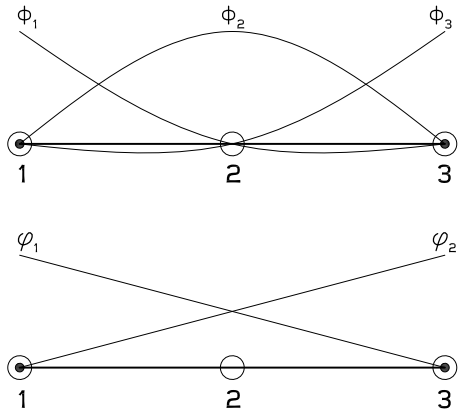

Figure 5: Lagrange polynomials as interpolation functions for displacements (top) and axial forces (bottom).

configuration and imposing a support displacement of $\Delta\mathbf{u} = (0, -7.93)$ m at the right support, as shown in Fig. 7.

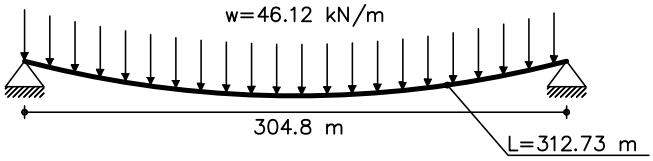

Figure 6: Structural Model for Example 1.

Property	**Value**
Cross-sectional area	548.4 mm^2
Elastic modulus	131.0 kN/mm^2
Cable self-weight	46.12 N/m
Cable length	312.73 m

Table 1: Geometric and Material Properties for Example 1.

Using a mesh of equal-size elements, Fig. 8 shows the maximum cable sag at midspan, as a function of the number of elements for both elastic

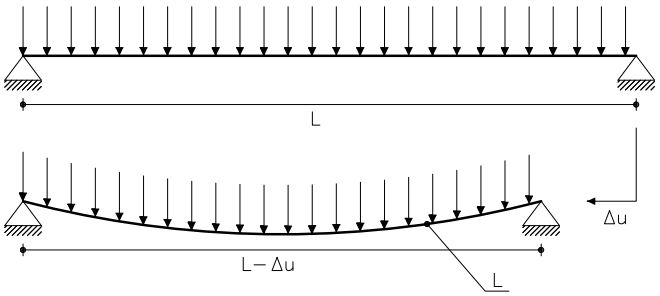

Figure 7: Form Finding Strategy for Example 1. According to Argyris et al. (1974).

material models in Section 6. The continuous and discontinuous formulations are compared to the corotational linear elastic truss element. A hyperbolic-cosine initial shape is assumed for the displacements as the starting guess of the Newton-Raphson iterative solution and a constant axial force of $15\,kN$ is assumed for the continuous formulation. Note that the solution for the corotational truss oscillates because of the absence of a node at midspan for an odd number of elements.

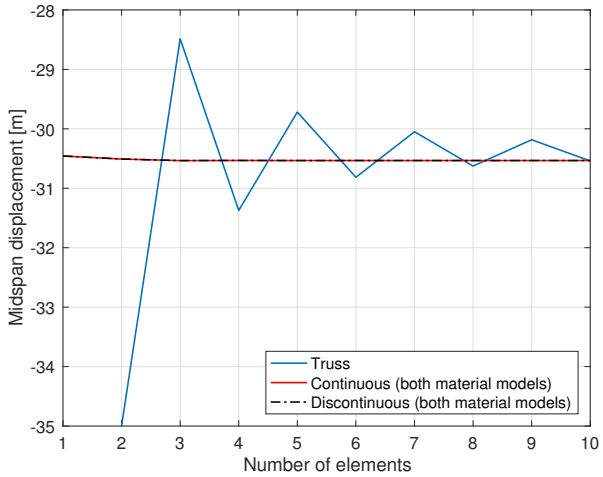

Figure 8: Maximum sag at midspan for both materials models and formulations, and for corotational linear elastic truss elements.

For a mesh of equal-size elements, the continuous and discontinuous formulations give identical results in Fig. 8. It is evident that the accuracy of the proposed elements is excellent even with a rather coarse mesh, in contrast

to the corotational truss which requires 10 or more elements for the cable. Both catenary elements give a midspan displacement of $y_{sv} = -30.5336$ m for a mesh of ten elements with the St Venant-Kirchhoff elastic material. The midspan displacement of both catenary elements for the same mesh is practically the same for the neo-Hookean elastic material at $y_{nh} = -30.5337$ m. In contrast, the midspan displacement for a mesh of ten corotational linear elastic truss elements is $y_t = -30.5404$ m.

Figure 9(a) shows the 2nd Piola-Kirchhoff axial force distribution along the cable for a mesh of equal-size elements and both material models and formulations. As is the case with Fig. 8, the discontinuous and the continuous cable elements and both material models give identical results. For a mesh with unequal-size elements that is generated by placing a node at 2/5 of the cable span and subdividing each portion into n equal-size elements, an inter-element discontinuity arises in Fig. 9(b) at the common node of elements with unequal size. The jump in the axial force value at the node located at 2/5 of the cable span reduces quickly with increasing number of elements and is very small for a mesh with 6 elements in Fig. 9(b).

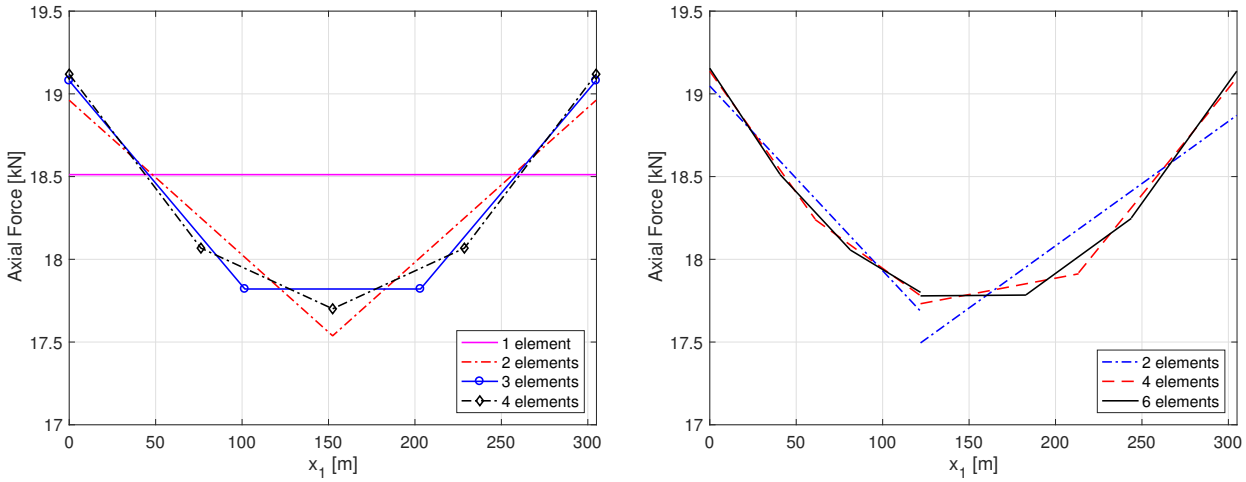

(a) Mesh with equal-size elements

(b) Mesh with unequal-size elements

Figure 9: 2nd PK axial force distribution; (a) both formulations and material models; (b) discontinuous formulation with both material models

While the response of the cable under self-weight in Fig. 8 and Fig. 9 is practically identical for the two elastic materials of Section 6, it is possible to

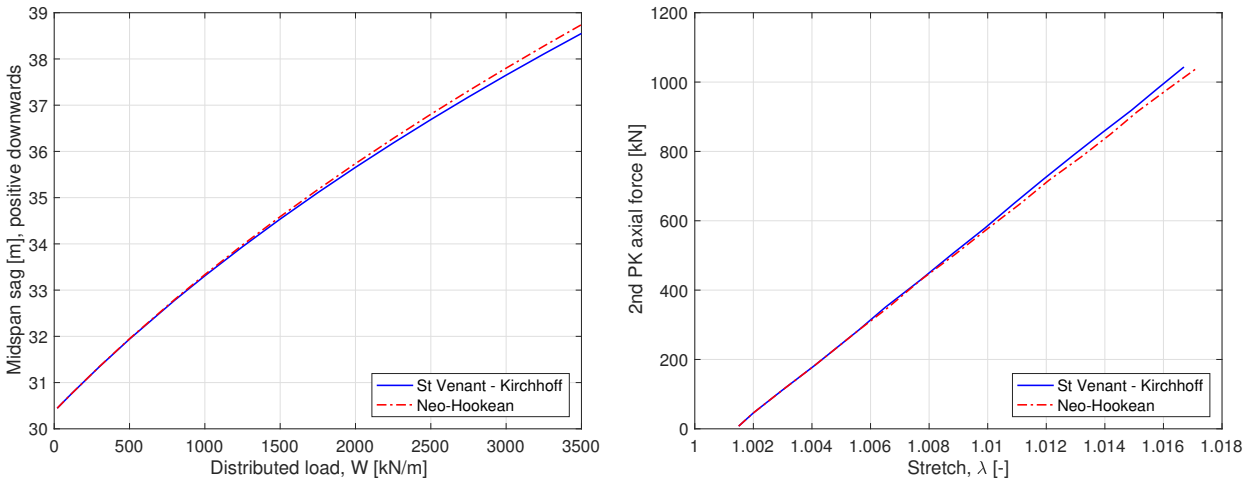

(a) Midspan sag vs. distributed load (b) 2nd PK axial force vs. stretch

Figure 10: Cable Response at midspan for Two Elastic Material Models.

detect response difference by increasing the distributed load value $W = \|\hat{\mathbf{W}}\|$. Fig. 10 shows the midspan sag and the 2nd PK axial force vs. the distributed load and stretch, respectively, with a mesh of four equal-size elements. As expected in small deformations, the relation between the midspan sag and the distributed load in Fig. 10(a) is initially linear and practically identical for the two material models, as is also the relation between the 2nd PK axial force and the stretch in Fig. 10(b). With increasing value of W, the St Venant-Kirchhoff elastic material gives smaller midspan sags and larger 2nd PK axial forces.

8.2. 2. Example: Cable under Self-Weight and Point Load

The second example deals with the same structural model as Example 1 under an additional concentrated load that is applied off-center, as shown in Fig. 11. This problem was subject of previous studies in Tibert (1999); Andreu et al. (2006); Thai and Kim (2011); Ahmad Abad et al. (2013), so that the results of different modeling can be readily compared. Fig. 11 and Table 1 summarize the geometry of the model and its material properties. The initial cable length between sections 1 and 2 in Fig. 11 is 125.88 m, while the initial cable length between sections 2 and 3 is 186.85 m. The applied concentrated force is 35.586 kN. The form finding problem is solved again with a horizontal reference configuration and a displacement $\Delta\mathbf{u} = (0, -7.93)$

m at the right support. The support displacement and the point load are applied simultaneously.

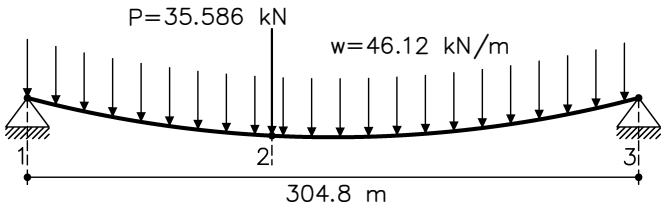

Figure 11: Structural model (case 2).

Figure 12 shows the deformed shape of the structure. Fig. 13 compares the sag and lateral drift of the cable at the point of the concentrated load application for the continuous and the discontinuous axial force distribution. The translation values are measured relative to the catenary shape from Example 1 and are practically the same for both elastic material models. Fig. 14 shows the 2nd Piola-Kirchhoff axial force distribution for the continuous and the discontinuous formulation. The advantage of the discontinuous axial force formulation is evident in Fig. 14(b): its ability to capture the jump in the axial force at the point of the concentrated load application results in the significantly better accuracy of the sag and lateral drift for coarse finite element meshes. In contrast, the continuous axial force formulation gives rise to the characteristic Gibbs phenomenon at the point of the concentrated load application as is evident from the axial force oscillation in Fig. 14(a).

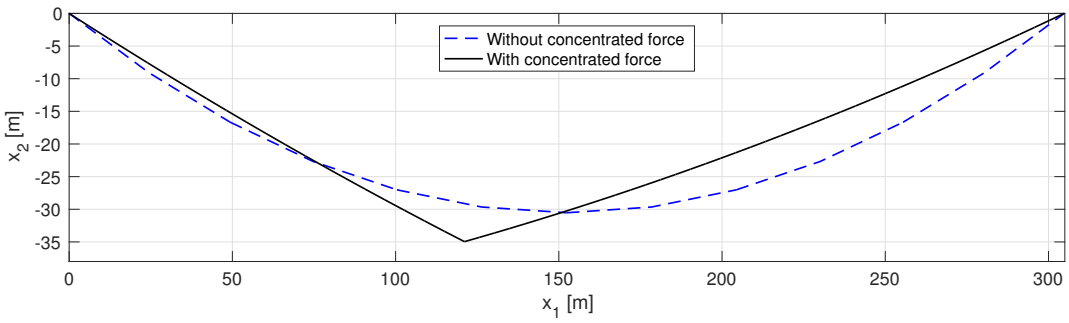

Figure 12: Converged deformed shape for case 2.

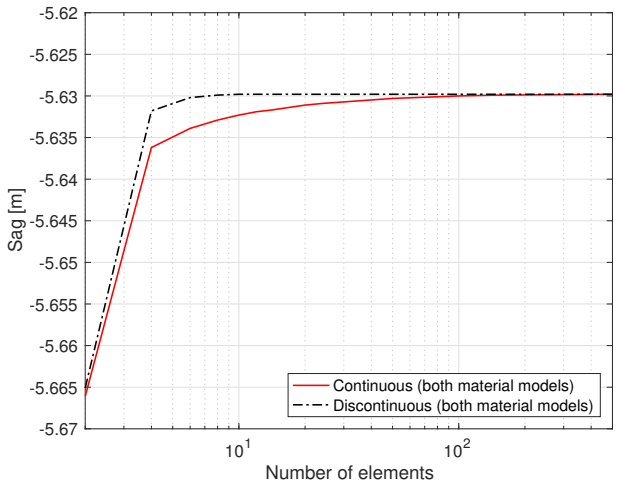

(a) Sag at point of load application

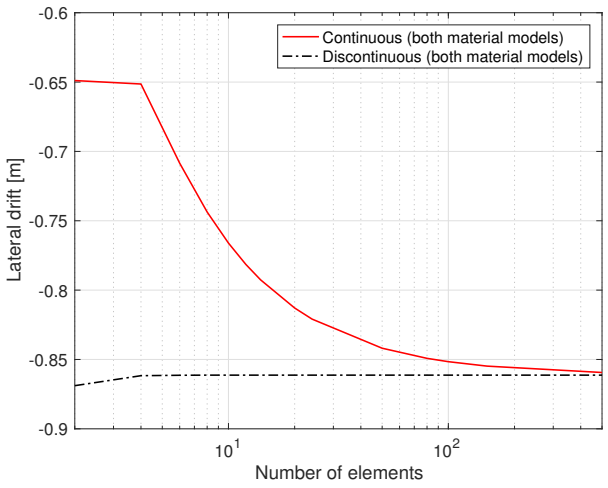

(b) Lateral drift at point of load application

Figure 13: Translations at the point of the concentrated load application relative to the deformed shape of the catenary for elastic material.

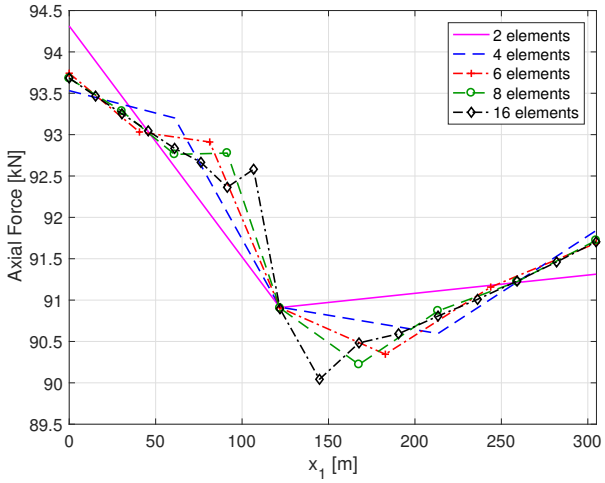

(a) Continuous axial force distribution

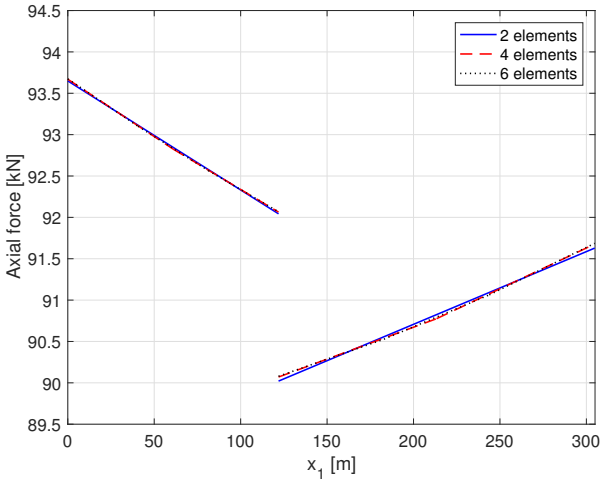

(b) Discontinuous axial force distribution

Figure 14: 2nd Piola-Kirchhoff axial force distribution for elastic material.

It takes a very fine finite element mesh to capture accurately the change in the axial force at the point of load application and to produce an accurate result for the translations at this point with the continuous formulation. In

fact, it takes more than 100 elements with the continuous formulation for the lateral drift to converge to the exact result in Fig. 13(b), while even two elements with the discontinuous formulation produce a value very close to the exact solution. No noticeable differences arise between the two elastic material models in Fig. 13 and Fig. 14. It is possible to eliminate the shortcoming of the continuous axial force formulation by linking only the cable displacements at the common node of adjacent elements, thus, in effect, allowing for a discontinuous axial force distribution with two independent axial force degrees of freedom at the common node.

Reference	**Element type**	**Vertical disp. (m)**	**Horizontal displ. (m)**
Michalos and Birnstiel (1962)	Truss	-5.472	-0.845
O'Brien and Francis (1964)	Elastic catenary	-5.627	-0.860
Jayaraman and Knudson (1981)	Truss	-5.471	-0.845
Jayaraman and Knudson (1981)	Elastic catenary	-5.626	-0.859
Tibert (1999)	Elastic catenary	-5.626	-0.859
Andreu et al. (2006)	Elastic catenary	-5.626	-0.860
Yang and Tsay (2007)	Elastic catenary	-5.625	-0.859
Thai and Kim (2011)	Elastic catenary	-5.626	-0.859
Ahmad Abad et al. (2013)	Discrete elastic catenary	-5.592	-0.855
Ahmad Abad et al. (2013)	Elastic catenary	-5.626	-0.859
Ahmad Abad et al. (2013)	Discrete elastic catenary with point loads	-5.830	-0.873
Present work (continuous, nonlinear elasticity)	Discrete elastic catenary, finite-deformations	-5.630	-0.861
Present work (discontinuous, nonlinear elasticity)	Discrete elastic catenary, finite-deformations	-5.630	-0.861

Table 2: Results for the Cable Model of Example 2 from different studies.

Table 2 compares the translation values of the present study with the results of several models in earlier studies. The agreement is excellent, even though the assumption of infinitesimal deformations in earlier studies appears to slightly underestimate the translation values. Another cause for the slight discrepancy is the lack of distinction between axial force representations in earlier studies and the assumption of a constant axial force along the cable in some.

8.3. 3. Example: Transport Pulley System

The third example investigates the stability of a cable supported by a pulley that was previously studied in Bruno and Leonardi (1999), Such et al. (2009) and Impollonia et al. (2011). Fig. 15 shows the structural model, consisting of an inclined cable that is anchored at both ends and supported by an intermediate roller. Table 3 summarizes the geometric and material properties of the structural model. The St Venant-Kirchhoff elastic material model is used for the cable.

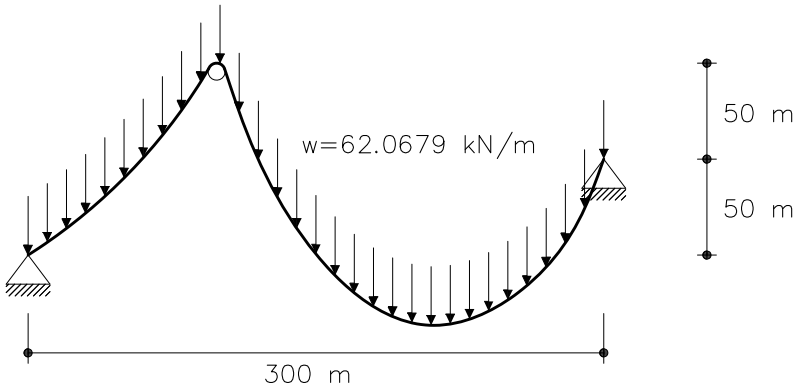

Figure 15: Structural model for Example 3.

The objective of this example is the determination of the equilibrium configurations of the cable under the assumption that the pulley is free to move horizontally and that the pulley radius is negligible. For the nonlinear analysis, the cable is subdivided in two segments, one for each span, with the curvilinear coordinate ξ^1 of the roller as problem unknown. The curvilinear coordinate ξ^1 refers to the arc-length in the reference configuration with origin at the left support, and is used to locate the roller node and subsequently

Property	**Value**
Cross-sectional area	805 mm^2
Elastic modulus	16.0 kN/mm^2
Cable self-weight	62.0679 N/m
Cable length	500 m

Table 3: Geometry and Material Properties for Example 3.

construct the finite element mesh. The analysis starts from a horizontal reference configuration and imposes a displacement of $\Delta\mathbf{u} = (-200, 50)$ m at the right support and a displacement of $\Delta u_2 = 100$ m at the intermediate roller. Moreover, the condition is imposed that the Cauchy axial force have zero jump at the roller support, as friction is neglected. As a result, the problem is solved by iterating over the curvilinear coordinate ξ^1 so that the jump in the Cauchy axial force at the roller becomes zero.

	Bruno and Leonardi (1999)	Such et al. (2009)	Impollonia et al. (2011)	Present work (continuous)	Present work (discontinuous)
ξ_1^1 (m)	111.07	110.96	110.83	110.83	110.83
N_1 (kN)	15.499	14.531	14.531	4.709 - 14.514	4.709- 14.515
ξ_2^1 (m)	-	-	221.52	221.53	221.51
N_2 (kN)	-	-	10.631	2.726 - 10.622	2.726 - 10.622
ξ_3^1 (m)	446.37	446.92	447.30	447.30	447.29
N_3 (kN)	17.952	17.966	17.982	5.222 - 17.960	5.222- 17.957

Table 4: Results for the Cable Model of Example 3 from different studies.

Table 4 summarizes the results for the equilibrium configurations by different authors with ξ_i^1 refering to the curvilinear coordinate of the pulley and N_i to the axial force. Because the studies in Bruno and Leonardi (1999), Such et al. (2009) and Impollonia et al. (2011) do not account for finite deformations, the corresponding values in Table 4 correspond to infinitesimal deformations. For the results of the present study the axial force corresponds

to the 2nd Piola-Kirchhoff axial force and the curvilinear coordinate to the reference configuration. While the values of the present study agree very well with those of previous studies, it is worth noting the variation of the axial force that the current formulation captures, as indicated by the range of axial force values for the cable in Table 4. In contrast, previous models overestimate the axial force by reporting a value corresponding to the maximum of the current formulation.

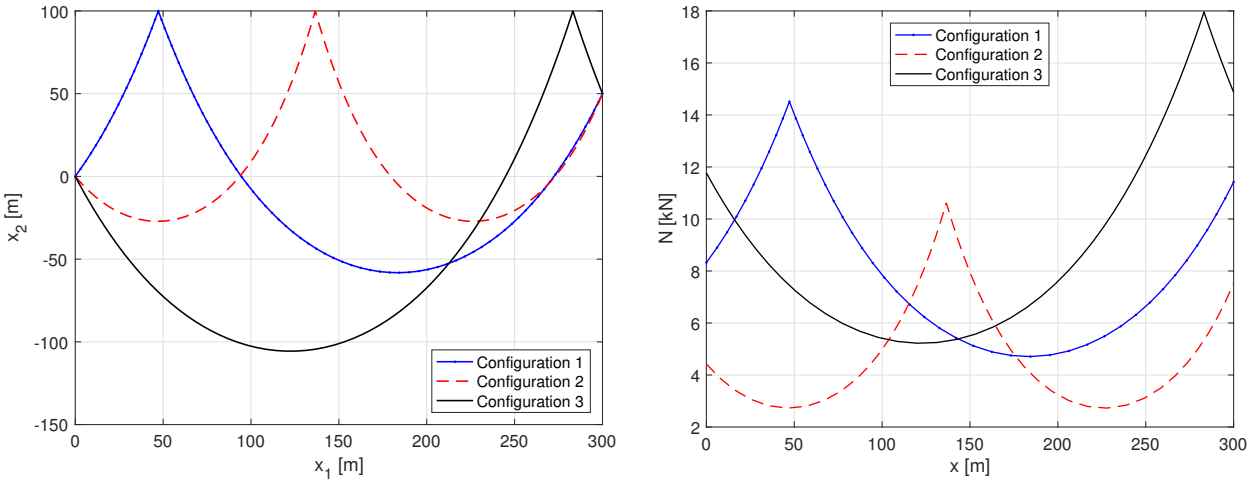

(a) Deformed shape (b) 2nd PK axial force distribution

Figure 16: Deformed shape of equilibrium states and 2nd PK axial force distribution for 45 equal-size elements.

Three equilibrium states result from the analysis, as Fig. 16(a) shows: two stable configurations, denoted with 1 and 3, and one unstable configuration, denoted with 2, as reflected by the change of direction for the horizontal component of the reaction at the pulley in Fig. 17, where the horizontal reaction equal to zero implies an equilibrium configuration. The stable configurations 1 and 3 are not symmetric, because the cable is inclined. The x_1 positions of the pulley for these equilibrium states in Fig. 16(a) are $x_1^1 = 47.253/47.253$ m, $x_1^2 = 136.540/136.533$ m and $x_1^3 = 283.155/283.144$ m for the continuous and the discontinuous formulations, respectively. Fig. 16(b) shows the 2nd Piola-Kirchhoff axial force distribution for the three equilibrium states. Both formulations produce the same result, as is also confirmed by the values in Table 4, because the axial force is continuous at the pulley in the absence of

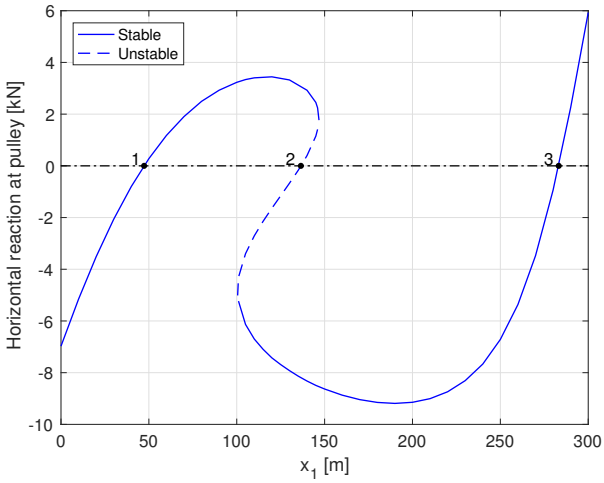

Figure 17: Horizontal reaction at pulley support vs. horizontal position x_1.

friction.

9. Conclusions

A new family of catenary elements based on finite deformations and a weakly-compatible mixed finite-element approach is presented. According to the weak statement of the nonlinear catenary problem, two types of catenary elements are derived: one with a continuous axial force distribution and one with a discontinuous axial force distribution.

The study derives the kinematics of the problem in general curvilinear coordinates and identifies the kinematic variables. Afterwards, the principle of virtual work and the weak form of the strain-displacement relationship are obtained. Finally, the finite-element implementation for the continuous and discontinuous elements is presented.

Three classical examples are used to assess the proposed formulation. These studies show that the continuous and discontinuous formulations give the same results for meshes of equal-size elements in symmetric problems. Moreover, they also show that a small number of elements is required for very accurate results. In contrast, the discontinuous formulation produces discontinuous axial force distributions when used in meshes of unequal-size elements and symmetric problems, with the results converging to the contin-

uous solution as the mesh is refined.

Under concentrated loads, the continuous formulation provides inaccurate results for coarse meshes, especially for horizontal displacements. In contrast, the discontinuous formulation intrinsically accommodates jumps in the axial force at the point of load application, and thus produces very accurate results for coarse meshes. The continuous formulation converges to the exact solution when the mesh is refined, despite the presence of Gibbs oscillations due to the nature of the approximation.

The proposed formulation can accommodate different material models. In this study, nonlinear elastic materials are discussed with the results confirming that St Venant-Kirchhoff and neo-Hookean materials behave robustly in both formulations. The two material models give practically identical displacements and axial forces for the same material stiffness EA under a small distributed load, as is expected for small deformations. Under increasing distributed load, the results show that a St Venant-Kirchhoff model gives smaller midspan sags and larger 2nd PK axial forces with respect to a neo-Hookean model.

The proposed catenary elements are able to identify the equilibrium configurations with significant accuracy, and distinguish stable from unstable states. For these equilibrium configurations, the accuracy of the resulting axial force distribution is noteworthy, in contrast to existing catenary elements which overestimate the axial forces because of their assumption of a constant axial force distribution.

In conclusion, because of their consistency, versatility and numerical robustness, the proposed catenary elements seem well suited for the analysis of nonlinear elastic cables under general loading.

10. References

Ahmad Abad, M. S., Shooshtari, A., Esmaeili, V., Riabi, A. N., 2013. Nonlinear analysis of cable structures under general loadings. Finite Elements in Analysis and Design 73, 11–19.

Ahmadizadeh, M., 2013. Three-dimensional geometrically nonlinear analysis of slack cable structures. Computers and Structures 128, 160–169.

Andreu, A., Gil, L., Roca, P., 2006. A new deformable catenary element for the analysis of cable net structures. Computers and Structures 84, 1882–1890.

Antman, S., 2005. Nonlinear Problems of Elasticity, 2nd Edition. Applied Mathematical Sciences. Springer.

Argyris, J. H., Angelopoulos, T., Bichat, B., 1974. A general method for the shape finding of lightweight tension structures. Computer Methods in Applied Mechanics and Engineering 3, 135–149.

Bishop, R., Goldberg, S., 1980. Tensor Analysis on Manifolds, 1st Edition. Dover Publications, Inc.

Brezzi, F., Bathe, K., 1990. A discourse on the stability conditions for mixed finite element formulations. Computer Methods in Applied Mechanics and Engineering 82, 27–57.

Bruno, D., Leonardi, A., 1999. Nonlinear structural models in cableway transport systems. Simulation Practice and Theory 7 (3), 207–218.

de Borst, R., Crisfield, M., Remmers, J., Verhoosel, C., 2012. Non-linear finite element analysis of solids and structures, 2nd Edition. John Wiley & Sons, Ltd.

Evans, L. C., 2010. Partial Differential Equations, 2nd Edition. American Mathematical Society.

Filippou, F. C., 2007. FEDEASLab - Finite Elements in Design, Evaluation and Analysis of Structures.
URL `http://www.ce.berkeley.edu/~filippou/Courses/FEDEASLab.htm`

Gurtin, M., 1982. An Introduction to Continuum Mechanics. Mathematics in Science and Engineering. Academic Press.

Haber, R. B., Abel, J. F., 1982a. Initial equilibrium solution methods for cable reinforced membranes. Part I: Formulations. Computer Methods in Applied Mechanics and Engineering 30, 263–284.

Haber, R. B., Abel, J. F., 1982b. Initial equilibrium solution methods for cable reinforced membranes. Part II: Implementation. Computer Methods in Applied Mechanics and Engineering 30, 285–306.

Hughes, T., 2000. The Finite Element Method. Linear Static and Dynamic Finite Element Analysis, 1st Edition. Dover Publications, Inc.

Impollonia, N., Ricciardi, G., Saitta, F., 2011. Statics of elastic cables under 3d point forces. International Journal of Solids and Structures 48, 1268–1276.

Jayaraman, H. B., Knudson, W. C., 1981. A curved element for the analysis of cable structures. Computers and Structures 14, 325–333.

Lacarbonara, W., 2013. Nonlinear structural mechanics. Springer.

Leonard, J. W., 1988. Tension structures. McGraw-Hill.

Michalos, J., Birnstiel, C., 1962. Movements of a cable due to changes in loadings. Transcripts of the American Society of Civil Engineers 127, 267–303.

O'Brien, W. T., Francis, A. J., 1964. Cable movements under two-dimensional loads. Journal of Structural Division ASCE.

Simo, J. C., Hughes, T. J. R., 1998. Computational Inelasticity, 1st Edition. Springer.

Steigmann, D. J., 1990. Tension-field theory. In: Proceedings of the Royal Society of London. Vol. 429 of Series A, Mathematical and Physical Sciences. pp. 141–173.

Such, M., Jimenez-Octavio, J., Carnicero, A., Lopez-Garcia, O., 2009. An approach based on the catenary equation to deal with static analysis of three dimensional cable structures. Engineering Structures 31, 2162–2170.

Taylor, R. L., 2014. FEAP - Finite Element Analysis Program. URL `http://www.ce.berkeley/feap`

Thai, H., Kim, S., 2011. Nonlinear static and dynamic analysis of cable structures. Finite Elements in Analysis and Design, 237–246.

Tibert, G., 1999. Numerical analysis of cable roof structures. Master's thesis, KTH.

Veenendaal, D., Block, P., 2012. An overview and comparison of structural form finding methods for general networks. International Journal of Solids and Structures 49, 3741–3753.

600 Yang, Y. B., Tsay, J. Y., 2007. Geometric nonlinear analysis of cable struc-
601 tures with a two-node cable element by generalized displacement control
602 method. International Journal of Structural Stability and Dynamics, 571–
603 588.

604 Zienkiewicz, O. C., Taylor, R. L., Fox, D. D., 2014. The Finite Element
605 Method for Solid and Structural Mechanics, 7th Edition. Elsevier, Ltd.